Characterization of reactant refill and detonation wave dynamics in a GOx/Natural-gas RDRE using simultaneous high repetition-rate OH-PLIF and chemiluminescence

Robert B. Wang*, Austin M. Webb†, Rafael D. Camacho‡, Mikhail Slipchenko§,
James Braun¶, Terrence R. Meyer‖, Venkat Athmananthan**
School of Mechanical Engineering, Purdue University, W. Lafayette, IN 47907, USA

Christopher A. Fugger††, Sukesh Roy‡‡
Spectral Energies LLC, Beavercreek, OH 45035, USA

Hugh D. Perkins§§
NASA Glenn Research Center, Cleveland, OH 43315, USA

The potential application of rotating detonation engines (RDEs) in rocket combustors hinges on a fundamental understanding of detonation wave structure and injector characteristics with fuel and oxidizer compositions relevant in rocket systems. Simultaneous 300 kHz-rate broadband OH* chemiluminescence and OH-PLIF imaging is employed in a fully optically accessible Natural Gas-GOx rotating detonation rocket engine (RDRE) to visualize reactant refill dynamics and detonation wave structure. A custom-built KTP-type optical parametric oscillator (OPO) is coupled with a nanosecond high-repetition-rate burst-mode laser to output 284 nm light and target excitation of the $Q_1(9)$ transition in the OH radical. Significant deflagrative burning is observed throughout the chamber as a consequence of the oxygen-rich environment. Trailing Azimuthal Reflected Shock Combustion (ARSC) system, similar to those in a H_2-air RDE are observed, burning unburned reactants in the region immediately following the primary detonation wave. Contact burning, as indicated in this study, does not seem to be a primary loss mechanism. The simultaneous measurement of OH and OH* show that axial locations exist in the refill process where OH radicals are present, and produced due to shear layer induced deflagration, however, these zones do not produce excited state OH*. While a deeper understanding of the underlying physics in RDRE systems requires further investigation, this work highlights a first-of-its-kind visualization of the turbulent combustion product field and reactant refill characteristics in this highly unsteady environment.

I. Introduction

The past several decades have seen a large rise in the interest of applying pressure gain combustion (PGC) as a replacement to modern constant-pressure combustors, particularly in rocket systems. Thermodynamic cycle analysis studies have shown the theoretical capability for PGC, which relies on a constant-volume detonative combustion process, to offer an approximately 20% increase in thermal efficiency compared to typical constant-pressure devices operating based on the Brayton cycle, which use slow deflagrative combustion to convert chemical energy into useful work [1, 2]. Several detonation-based engine architectures have been proposed, with the most promising and widely researched concept being the rotating detonation engine (RDE). The RDE enables continuous uninterrupted operation by feeding

*Doctoral Student, School of Mechanical Engineering
†Doctoral Student, School of Mechanical Engineering
‡Doctoral Student, School of Aerospace and Aeronautics
§Research Associate Professor, School of Mechanical Engineering
¶Research Assistant Professor, School of Mechanical Engineering
‖Professor, School of Mechanical Engineering and School of Aerospace and Aeronautics (by Courtesy)
**Research Scientist, School of Mechanical Engineering
††Research Engineer
‡‡Senior Research Engineer
§§Aerospace Engineer

propellants along the axial length of an annular combustor, allowing a detonation wave to propagate circumferentially around the annulus so long as reactants are being supplied. Another detonation-based engine concept is the pulsed detonation engine (PDE), in which reactant mixture is ignited at the head-end of a detonation channel and the detonation wave propagates linearly until it is eventually exhausted out to the surroundings. However, the design of the PDE necessitates reactant refill and reignition at high frequencies in order to provide a constant thrust profile, which limits this system to the mechanical capabilities of the fluid components and ignition source. In an RDE, these limitations are circumvented by allowing the detonation wave to travel around the combustion channel of an RDE at frequencies on the order of several kilohertz with a single ignition at start-up [3]. Additionally, RDE architectures feature a compact constant-volume design, enabling simple yet effective conversion of chemical energy into kinetic energy and useful work output. While considerable work has been accomplished experimentally and numerically to characterize PDE and RDE performance and detonation wave characteristics [1, 4–7], significant challenges still hinder development of PGC as a viable replacement to modern-day deflagrative combustors as net pressure gain in an RDE has yet to be seen in the open literature.

To fully understand the complex RDE flow-field, a large effort has been dedicated to optimizing injector design and investigating injector dynamics [8, 9], studying reactant mixing and the effects of deflagration ahead of the detonation wave on the operability [10–13], and analyzing the heat transfer and implementing cooling schemes to handle the large thermal loads present in RDEs [14, 15]. In the analysis of the observed deflagration, there are inconsistencies in the explanations. Conventionally, the deflagration preceding the detonation wave is ascribed to the mixing of hot products and cold reactants in local recirculation zones. Additionally, contact burning is attributed to the reactant refill process, involving direct contact between incoming fresh reactants that expel product gases outward [13].

However, a significant inconsistency arises from the fact that the physical processes of mixing and reactant expulsion occur on significantly faster time scales ($\approx 100 - 300\mu$s) compared to the autoignition delay time of reactants, typically on the order of 1-5 μs (for reactants in the shear layer at 800 - 1200 K) [12, 16]. This raises the question of whether the deflagration ahead of the detonation wave is genuinely caused by fresh reactants or if it is simply the presence of long-lived OH radicals.

To address this inconsistency, laser-based diagnostics can be employed to detect the production of OH radicals. This approach can help resolve the question of the presence of contact deflagration as well as shear-layer-induced deflagration in local recirculation zone pockets, as proposed by [13]. Consequently, this study presents the first experimental evidence of the presence of deflagration ahead of the detonation wave, a phenomenon typical in oxygen-rich environments. Notably, this phenomenon is not observed in a 1-to-1 configuration that the same combustor was operated at for an H2-Air combination of propellants.

Laser-based and general optical diagnostics such as chemiluminescence imaging, planar laser-induced fluorescence (PLIF), laser absorption spectroscopy (LAS), and coherent anti-Stokes Raman scattering (CARS) allow for visualization of the turbulent combustion product field and non-intrusive in-situ measurements of temperature and species concentration, and considerable work has been accomplished in the development of these techniques in RDE environments for gas phase reactants and most commonly for air-breathing RDEs with gaseous H_2 as fuel [8, 17–19]. Further understanding of the complex physics of RDEs in air-breathing and rocket systems for propulsion applications requires a transition from gaseous reactants to liquid fuels and, in the rocket case, liquid oxidizers. However, there are substantial challenges in applying non-intrusive laser-based measurement techniques in condensed phase detonation environments, including optical access limitations, judicious selection of a propellant/tracer with an accessible molecular excitation wavelength, and laser repetition rate and energy. Additionally, in the liquid fuel-gaseous oxidizer case, it is important to study both the condensed phase and gas phase flow fields and their interaction, which itself presents significant difficulties. As a step towards applying diagnostics to full liquid fuel RDEs, previous studies in our group investigated the one-way coupled interaction between a detonation wave and a single liquid diesel fuel jet in a H_2-air RDE and characterized liquid injection refill and recovery dynamics using MHz rate diesel PLIF with an excitation wavelength of 355 nm, outputted from a burst-mode laser system built in-house [8, 20]. This work focuses on applying laser diagnostics in rocket-type combustors by taking OH-PLIF images at 300 kHz in an RDRE operating with gaseous CH_4 and gaseous oxygen as propellants. This is accomplished using an optical parametric oscillator (OPO) that outputs 284 nm light to target the $Q_1(9)$ transition in the OH radical. Simultaneously, OH* chemiluminescence images are taken to correlate the OH-PLIF data with the location of the detonation wave relative to the PLIF plane and study reactant refill dynamics and deflagrative burning in the channel.

II. Experimental Setup and Methodology

A. RDE Test Platform

Details of the RDRE test platform can be found in our prior work [21]. The experimental change occurs with modification of the source of propellants that provides gaseous oxygen to be supplied as oxidizer and Natural-gas as fuel. Geometric parameters are provided here for continuity. The RDRE, termed REAPR (RDE Experimental Apparatus for Polyfuel Rockets), a modification from our prior work THOR [11], has an outer diameter of 136 mm and a chamber channel height of 10.7 mm. Gaseous Oxygen flows through a converging-diverging section with a throat gap of 1.42 mm. At a supersonic area ratio $\epsilon = 1.18$, where the free-stream Mach number is approximately 1.8, fuel is injected as a jet-in-crossflow through 100 orifices spaced evenly around the azimuth, with each orifice milled with an end-mill of 0.6 mm to a depth of 0.4 mm. At $\epsilon = 1.81$, the expansion increases abruptly to ~7 by a backward-facing step (BFS). Fuel and oxidizer are both metered using critical flow venturis with a flow rate uncertainty of ~2%. A schematic representation of the chamber geometry is shown in Fig. 1. For these tests, the RDE is run at the stochiometric OF ratio of 4.0, with a GOx mass flow rate of 1 lbm/s and a CH_4 mass flow rate of 0.25 lbm/s.

As a modular system, REAPR can be tested with both a 20 mm thick fused silica quartz outer-body as well as an instrumented metal outer-body constructed from SS316. The instrumented outer-body enable low-frequency (5 kHz) pressure measurements using GE UNIK5000 pressure transducers with a capillary-tube attenuated pressure (CTAP) arrangement. Low-frequency static temperature data is collected with thermocouples, and several ports on the instrumented outer-body allow for high-frequency pressure transducers (PCB 113B21, 0–200 psia) to be flush-mounted at various azimuthal and axial locations along the combustor. To enable seamless data acquisition and control during each hot-fire, all sensors and measurements are triggered at the start of the process through a data acquisition and control system (DACS). This DACS serves for condition monitoring and controlling the operation of the rocket engine (RDE). The entire experiment is automated, incorporating precise timing for activities such as valve operations, pre-detonation ignition, engine firing, and engine shutdown.

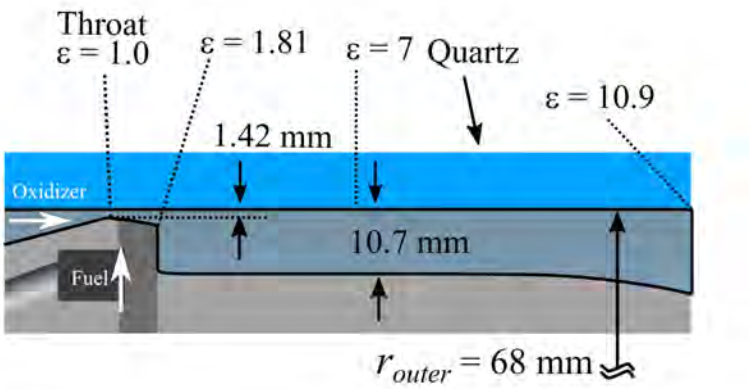

Fig. 1 Schematic of the radial-axial cross section of the flow path (reprinted from [12] with permission from the authors).

This manuscript primarily centers on a singular experimental baseline condition. Although sweeps were conducted across various conditions, the fundamental physics governing the propagation of the rotating detonation in the RDRE case exhibited consistent behavior. Consequently, the baseline operating condition was chose with an oxidizer throat mass flux of $G_{ox} = 350 kg/m^2/s$ at a global equivalence ratio of $\phi = 1.0$ or an O-F ratio of 4.0. While experiments with O-F ratios of 3 and 5 were conducted, it's important to note that the overarching physics discussed in this work remained consistent across these variations.

B. OH-PLIF and Chemiluminescence Setup

The quartz outer-body provides the necessary optical access to permit high-speed imaging of chemiluminescence from the detonation wave as well as fluorescence from laser-based excitation of target molecules in the chamber, as in the PLIF images captured in this work. Readers are directed to [22] for details on the layout and configuration of the tunable OPO used to generate the requisite 284 nm light. In this work, the output 284 nm beam is measured to have

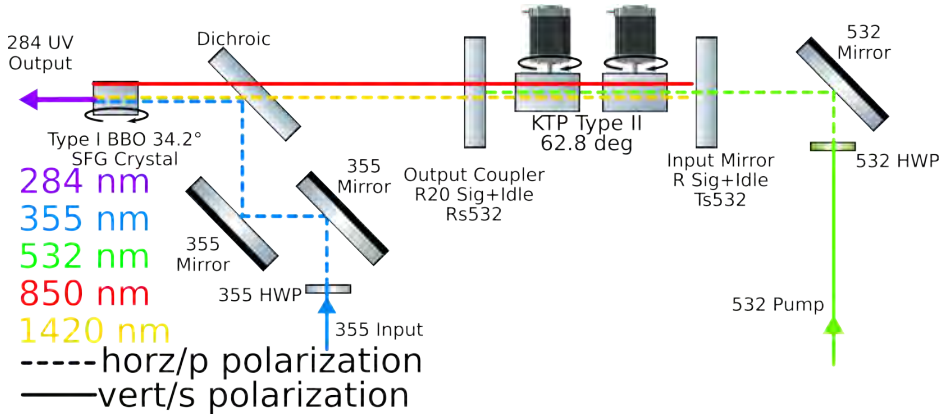

Fig. 2 Schematic of the KTP-OPO for probing a range of target molecules including the hydroxyl radical, OH.

~300 μJ/pulse at 300 kHz to excite the target OH transition. The beam is then routed to the test cell and focused down to the channel of REAPR. A Shimadzu HPV-X2 coupled to a Lambert Instruments UV HiCatt image intensifier with a 320 ± 20 nm band-pass filter to capture the OH fluorescence signal at approximately 310 nm. The intensifier is gated down to 10 ns to suppress the background OH* chemiluminescence from the PLIF image. A Phantom TMX 7510 is coupled to a Lambert Instruments UV-Visible HiCatt intensifier to capture the OH* chemiluminescence from the detonation wave, with a gate width of 100 ns. The chemiluminescence FOV is reflected off of two UV-enhanced aluminum mirrors to allow for simultaneous OH-PLIF and chemiluminescence. A schematic of the OH-PLIF setup is shown in Fig. 3.

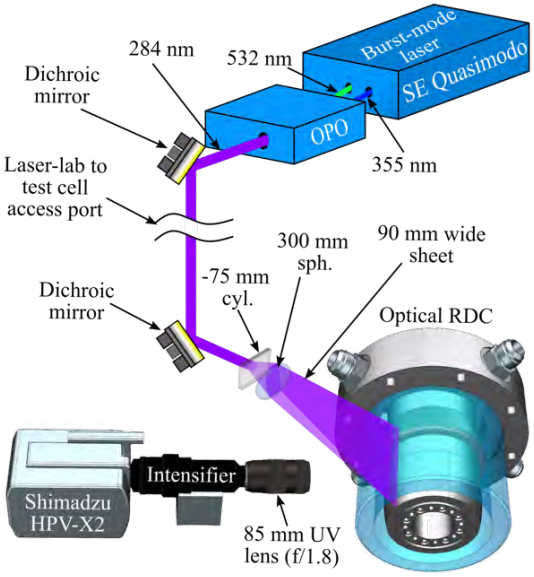

Fig. 3 Setup for the 300 kHz OH-PLIF imaging.

III. Results and Discussion

The Results section is organized into three parts. The initial section offers a comprehensive overview of the detonation structure observed in the $\theta - x$ direction, as captured by the high-speed camera. The second part delves into the propagation physics of the detonation wave under the baseline operating condition, using the 300 kHz imaging from the OH* chemiluminescence camera. Notably, low levels of OH* were observed during the refill process, posing the question of whether the observed deflagration is associated with contact surface interactions. To answer these questions, the final section employs simultaneous orthogonal chemiluminescence ($\theta - x$) and PLIF imaging ($r - x$), providing three-dimensional insights. This approach reveals the origin of OH radicals and, notably, the experiment sheds light

on the levels of deflagration observed in an oxygen-rich environment. The section addresses the crucial question of whether contact surface deflagration truly exists, or if the OH* observed in the chemiluminescence camera stems merely from the product gases produced in the previous cycle. Furthermore, the last section aims to clarify the underlying inconsistencies concerning the nature and origin of deflagration in these environments.

A. Detonation Structure Description

The baseline condition detonation wave behavior is described in brief. The velocity of the detonation wave was observed to be approximately 2280 m/s (or 2.28 mm/μs), which is approximately 95% of the Chapman-Jouget velocity (C-J). This was determined using high-frequency pressure transducer measurements and cross-correlation analysis of high-speed chemiluminescence images, similar to prior work [11]. For the analysis of detonation wave structure under the baseline condition, a single image was selected using the 300 kHz OH* chemiluminescence, capturing the wave as it enters the camera's field of view (FOV). The camera exposure was set at 100 ns, during which the detonation wave moved approximately 0.228 mm. This movement is an order of magnitude lower than prior and first visualization of the detonation wave [23], where the detonation wave traveled around 5-10 mm during the camera exposure. The freeze-frame nature of the imaging setup ensures a true isolation of the flame front, eliminating smearing effects.

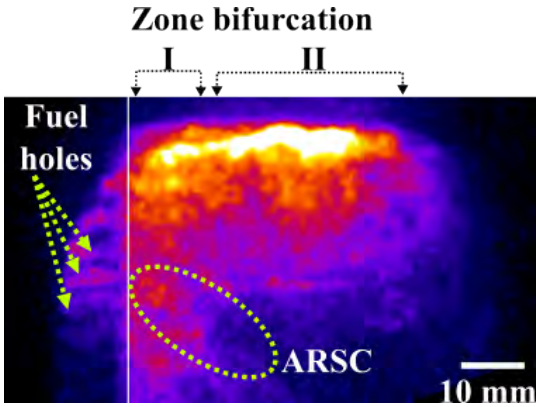

Fig. 4 Detonation wave structure of the Natural-Gas/GOx at the baseline condtion. Note that detonation wave is bifurcated into two zones I and II, similar to the experimental results observed in the H_2/Air case.

The detonation wave front indicates a noticeable zone separation in the axial direction, with the injection nearfield (Zone I) having low luminosity at the leading front, and the injection farfield (Zone II) having a higher luminosity at the leading front. This separation is attributed to (a) low static properties and (b) poor mixing in the injection nearfield, in contrast with the high static properties and better mixing in the injection farfield. The converging-diverging oxidizer inlet results in the supersonic injection of reactants ahead of the detonation wave, similar to our prior work on H_2-air conducted in the same combustor [12, 24].

Furthermore, in the injection nearfield, the trailing Azimuthal Reflected Shock Combustion system (ARSC) is observed. The combination of low-static quantities and poor mixing in this region results in the incomplete consumption of all reactants at the leading detonation front. Hence, vitiated unburned reactants pass through the leading detonation wave and undergo shock-induced combustion in the trailing azimuth shock system behind it. In Zone II, where better-mixed reactants with higher static quantities prevail, a significantly larger fraction of reactants at the leading front is consumed, leading to the absence of ARSC extension in the injection farfield. Detailed discussions on the origin of the ARSC phenomenon can be found in the authors' previous work [12].

Additionally, natural gas fuel jets are visible in this image, unlike the prior hydrogen-air case [24]. This visibility suggests that the detonation wave wake has a higher pressure compared to the H_2/Air case (approximately 2× based on C-J computations), resulting in a more pronounced backflow of burned gas.

In the next section, we'll delve into the mechanics of how the detonation wave propagates, using the information gathered from the 300 kHz chemiluminescence images.

B. Detonation Propagation Physics (300 kHz)

An image sequence of 60 images from the OH chemilumienscence is shown in Fig. 5. The image sequence is spaced at 3.33 μs and shows $\approx$ 2 cycles of the detonation wave passage. The frame of each image is 82×48 mm respectively,

providing the scale of the images presented. Additionally, phosphorescence due to the PLIF laser sheet, from the quartz glass used in this study, allows for a direct visual demarcation of the azimuthal location of the PLIF plane.

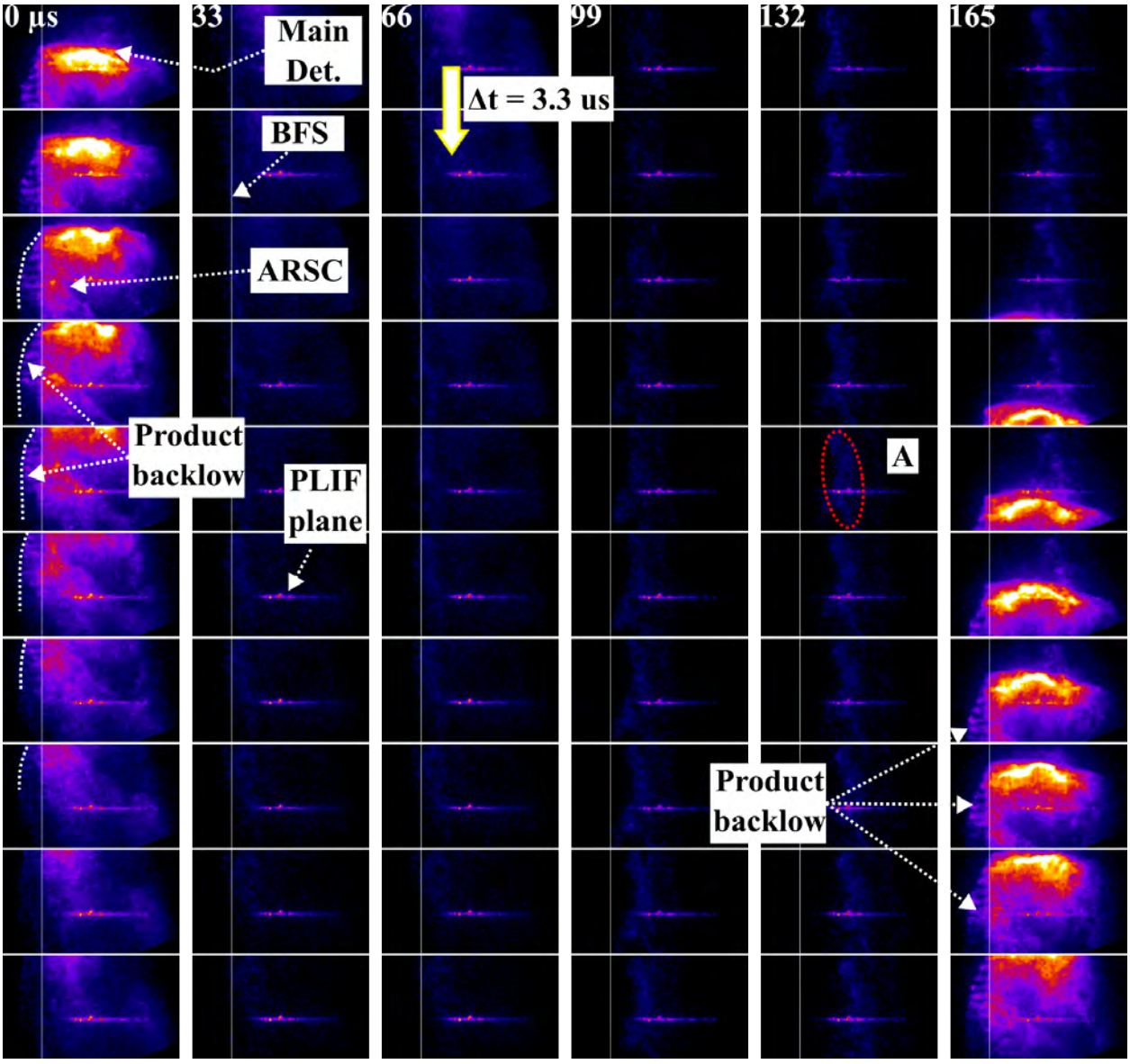

Fig. 5 OH Chemiluminescence images of detonation wave propagation at 300 kHz for 60 frames is shown. The image interval in the vertial direction is 3.33 μs and in the horizontal direction is 33 μs respectively. The T

As mentioned in the previous section, the detonation wave exhibits axial variation in Zone I and II, with a notable zone bifurcation leading to ARSC shock-induced detonation in the injection nearfield. Despite a high injector of $\frac{\Delta P}{P_{cc}}$ > 2.0, where Δ_P is the differential pressure between the plenum and combustion chamber and P_{cc} is the chamber pressure, the higher pressure in the wake of the detonation wave results in a significant backflow of burned gas.

A low-level chemiluminescence signal is observed between 66 – 165 μs during the refill process forming a contact boundary between cold reactants (absence of OH* - in the injection nearfield) and hot-products (presence of OH* in the far-field). This signals indicates the presence of OH at the contact point of the entering reactants and the product gas from the previous cycle exiting the system.

It is important to note that the presence of OH* does not necessarily imply the production of OH* (deflagrative heat release), which would indicate 'contact burning' prior to wave arrival and, potentially, be a major contributing loss

factor. However, as shown in the figure, the absence of an increase in OH* levels at the contact surface (Annotation A in Fig. 5) indicates a relatively subdued presence of contact surface deflagration as a loss mechanism. Further investigation using the OH-PLIF and the simultaneous orthogonal OH* chemiluminescence will be considered in the next section for furthe insights.

C. OH-PLIF of the detonation wave and refill process

Fig. 6 shows a 300 kHz image sequence of the OH flow field in the $r - x$ direction providing the radial slice during the entire detonation wave cycle. At t = 0 μs, we observe the presence of OH in the backward facing step, with admission of fresh reactants from the injector.

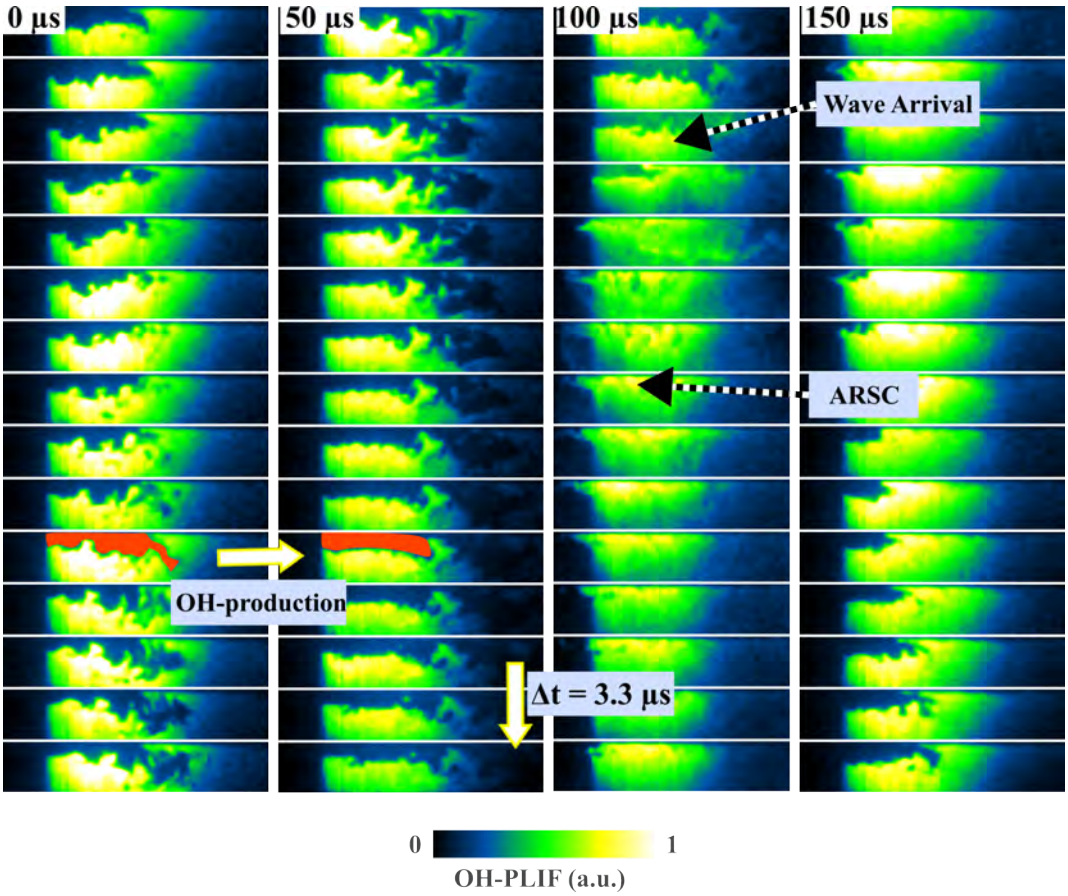

Fig. 6 300 kHz image sequence of the OH-PLIF signal observed from the PLIF camera. The images presented have indications of 1 full cycle with the detonation wave arriving at 110 μs.

he presence of OH indicates the existence of hot products, either from the wake of the detonation wave or from reactions occurring between the incoming reactants and the hot products. Conversely, the absence of OH during the RDE operation can be attributed to cold reactants entering the RDE—an extrapolation based on the assumption that the only cold medium in the RDE is the incoming fresh reactants.

As time progresses and refill occurs, a complex shear layer front with multiple features resembling vortex shedding becomes apparent between the incoming fresh reactants and the products of the previous cycle. Notably, as time advances, voids of OH—indicative of 'cold reactants'—begin to fill with OH radicals. This phenomenon can be attributed to two factors: (1) entrainment of hot products by the cold reactants and (2) the production of OH due to the mixing and local autoignition of the cold incoming fresh reactants. Nevertheless, it is evident that OH is indeed produced in the injection nearfield with the admission of fresh reactants. At approximately. At $\approx 109\mu$s, he wave reaches the PLIF plane. Subsequently, there is further OH production due to the ARSC combustion zone, although it is challenging to observe this ARSC compared to the hydrogen-air case [12]. It is also interesting to note that during the

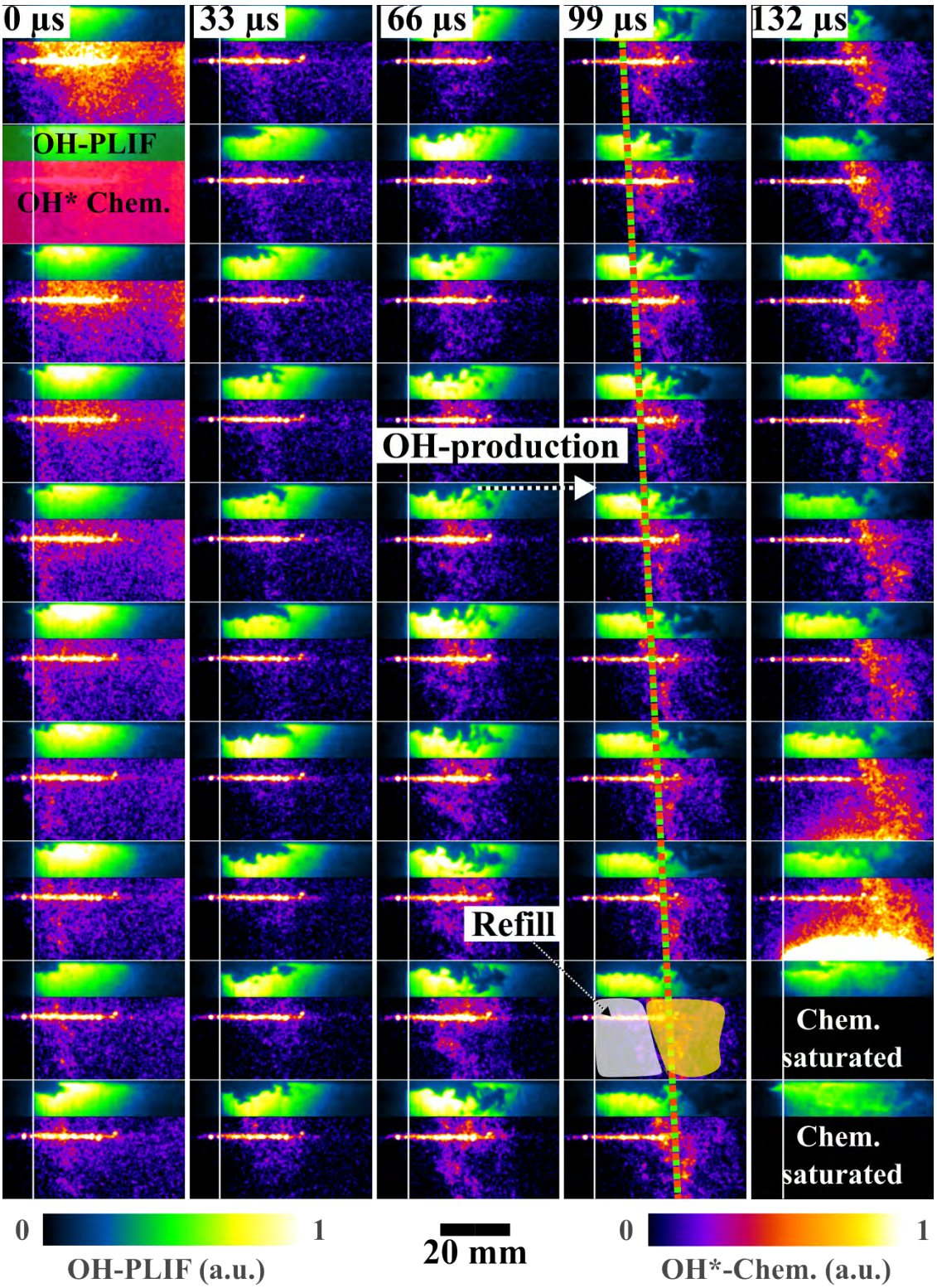

Fig. 7 300 kHz simultaneous orthogonal imaging of the OH-PLIF (top) and OH* chemiluminescence (bottom) during the refill process.

entire refill process, no OH-production was observed at th contact zone, indicating potentially the presence of either uncombustible reactants or low local autoignition delay times of the fresh incoming reactants.

Post wave passage, the product gases are observed entering upstream of the BFS and into the plenum. This product gas backflow is also noticeable in the chemiluminescence images, as depicted in Fig. 4 and Fig. 5. Around $\approx 150\mu$s, the reactants are observed being pushed outward, marking the commencement of the refill process for the next cycle.

While both the PLIF and chemiluminescence images indicate the presence of OH and OH*, respectively, the question of substantial evidence for contact surface deflagration remains intriguing. A more comprehensive understanding necessitates further investigation through simultaneous orthogonal measurements to paint a complete picture.

Fig. 7 shows the simultaneous orthogonal imaging of the OH* chemiluminescence ($\theta - xplane$) and OH-PLIF ($r - xplane$) and provides the 3D information on the detonation wave structure. The time sequence selected is aimed towards understanding the contact deflagration zone observed in the chemiluminescence. The azimuth location of the PLIF imaging is observed as a straigh line, due to the phosphoresence from the quartz glass, as mentioned earlier.

The chemiluminescence and PLIF images were median filtered and the chemiluminescence images were scaled up by a factor of $\times 10$ in order to visualize the low level deflagration that forms the contact layer.

Evident from out previous discussion, the low level deflagration observed starts to advect downstream, from 33μs onwards iwth increasing reactant refill. As the refil process progresses, OH is observed in the injection nearfield through out the refill, however OH* is absent. At $\approx 99\mu$s, presence of OH in the injection nearfield and absence of OH* at the same axial location, near the BFS is evident. This OH signal presence could potentially be attributed to shear layer-induced local deflagration of the reactants and the product gases. However, in the PLIF image, there is no distinct zone at the periphery demarcating the 'OH-contact' zone.

This observation is crucial for two reasons: Firstly, relying solely on conclusions drawn from OH* chemiluminescence for assessing deflagration levels may be insufficient. OH, being a reaction intermediate that tracks flames, can be present in locations where the excited state OH* may not be detected and is typical of only high temperature reaction locations (> 1500K). Secondly, there is no observable evidence of OH production at the contact between hot products and cold reactants at the axial refill height end. This indicates that the significance of contact burning as a major loss mechanism might need to be de-emphasized, as other competing and confounding effects could impact the RDE performance and operation.

IV. Conclusions

This preliminary investigation provides a detailed visualization of the turbulent combustion product field within a Rotating Detonation Rocket Engine (RDRE) environment. The broad conclusion are as follows:

- The investigation revealed axial variations in the detonation wave structure, notably in Zones I and II, with a distinctive zone bifurcation leading to the emergence of the Azimuthal Reflected Shock Combustion system (ARSC) in the injection nearfield.
- The analysis of the simultaneous orthogonal OH-PLIF and OH* chemiluminescence images provided valuable insights into the detonation wave refill process. The observation of low-level deflagration downstream during the refill suggested potential local deflagration induced by shear layers between reactants and product gases.
- The detection OH in the injection nearfield near the BFS, while concurrently observing the absence of OH* at the same axial location, suggests potential differences in temperature between the 'shear layer induced' deflagration and the hot products from the previous cycle. This discrepancy prompts a crucial inquiry into the reliability of OH* chemiluminescence measurements as a tool for assessing deflagration, whether ahead of the wave or at the contact surface.
- This discrepancy also emphasizes the importance of simultaneous orthogonal measurements for a comprehensive understanding of the combustion processes in RDREs.
- Ultimately, these findings challenge the assumption of contact burning as a major loss mechanism, and aims to shift focus on other competing and confounding effects may influence the RDRE performance and operation.

Acknowledgments

The primary author would like to acknowledge support from the National Defense Science and Engineering (NDSEG) Fellowship Award. Additionally, this work was funded in part by a NASA SBIR program.

References

[1] Raman, V., Prakash, S., and Gamba, M., "Nonidealities in Rotating Detonation Engines," *Annual Review of Fluid Mechanics*, Vol. 55, No. 1, 2023, pp. 639–674. https://doi.org/10.1146/annurev-fluid-120720-032612, URL https://doi.org/10.1146/annurev-fluid-120720-032612.

[2] J. Shaw, I., A.C. Kildare, J., J. Evans, M., Chinnici, A., A.M. Sparks, C., N.H. Rubaiyat, S., C. Chin, R., and R. Medwell, P., "A Theoretical Review of Rotating Detonation Engines," IntechOpen, 2021.

[3] Anand, V., and Gutmark, E., "Rotating detonation combustors and their similarities to rocket instabilities," *Progress in Energy and Combustion Science*, Vol. 73, 2019, pp. 182–234.

[4] Bykovskii, F. A., Zhdan, S. A., and Vedernikov, E. F., "Continuous Spin Detonations," *Journal of Propulsion and Power*, Vol. 22, No. 6, 2006, pp. 1204–1216. https://doi.org/10.2514/1.17656, URL https://doi.org/10.2514/1.17656.

[5] Kailasanath, K., Gupta, A. K., De, A., Aggarwal, S. K., Kushari, A., and Runchal, A., *Recent Developments in the Research on Pressure-Gain Combustion Devices*, Springer Singapore, Singapore, 2020, pp. 3–21.

[6] Ma, J. Z., Luan, M.-Y., Xia, Z.-J., Wang, J.-P., Zhang, S.-j., Yao, S.-b., and Wang, B., "Recent Progress, Development Trends, and Consideration of Continuous Detonation Engines," *AIAA Journal*, Vol. 58, No. 12, 2020, pp. 4976–5035.

[7] Zheng, Q., sheng Weng, C., and dong Bai, Q., "Experimental Research on the Propagation Process of Continuous Rotating Detonation Wave," *Defence Technology*, Vol. 9, No. 4, 2013, pp. 201–207.

[8] Hoeper, M. W., Webb, A. M., Athmanathan, V., Wang, R. B., Douglas Perkins, H., Roy, S., Meyer, T. R., and Fugger, C. A., "Liquid fuel refill dynamics in a rotating detonation combustor using megahertz planar laser-induced fluorescence," *Proceedings of the Combustion Institute*, 2022. https://doi.org/https://doi.org/10.1016/j.proci.2022.07.230, URL https://www.sciencedirect.com/science/article/pii/S154074892200267X.

[9] Teasley, T. W., Protz, C. S., Larkey, A. P., Williams, B. B., and Gradl, P. R., "A Review Towards the Design Optimization of High Performance Additively Manufactured Rotating Detonation Rocket Engine Injectors," *AIAA Propulsion and Energy 2021 Forum*, 2021. https://doi.org/10.2514/6.2021-3655.

[10] Ayers, Z. M., "Reactant Mixing Effects in Rotating Detonation Engines," Ph.D. thesis, 2023.

[11] Athmanathan, V., "Investigation of Rotating Detonation Combustion Dynamics using advanced in-situ Optical Diagnostics," Ph.D. thesis, 2021.

[12] Athmanathan, V., Braun, J., Ayers, Z. M., Fugger, C., Webb, A. M., Slipchenko, M. N., Paniagua, G., Roy, S., and Meyer, T. R., "On the effects of reactant stratification and wall curvature in non-premixed rotating detonation combustors," *Combustion and Flame*, 2022.

[13] Sato, T., Chacon, F., White, L., Raman, V., and Gamba, M., "Mixing and detonation structure in a rotating detonation engine with an axial air inlet," *Proceedings of the Combustion Institute*, Vol. 38, No. 3, 2021, pp. 3769–3776. https://doi.org/https://doi.org/10.1016/j.proci.2020.06.283, URL https://www.sciencedirect.com/science/article/pii/S1540748920303758.

[14] Braun, J., Sousa, J., and Paniagua, G., "Numerical Assessment of the Convective Heat Transfer in Rotating Detonation Combustors Using a Reduced-Order Model," *Applied Sciences*, Vol. 8, No. 6, 2018. https://doi.org/10.3390/app8060893, URL https://www.mdpi.com/2076-3417/8/6/893.

[15] Stevens, C. A., Fotia, M., Hoke, J., and Schauer, F., "Quasi Steady Heat Transfer Measuments in an RDE," *2018 AIAA Aerospace Sciences Meeting*, 2018. https://doi.org/10.2514/6.2018-1884.

[16] Stechmann, D. P., Sardeshmukh, S., Heister, S. D., and Mikoshiba, K., "Role of Ignition Delay in Rotating Detonation Engine Performance and Operability," *Journal of Propulsion and Power*, Vol. 35, No. 1, 2019, pp. 125–140. https://doi.org/10.2514/1.B37117.

[17] Rankin, B. A., Richardson, D. R., Caswell, A. W., Naples, A. G., Hoke, J. L., and Schauer, F. R., "Chemiluminescence imaging of an optically accessible non-premixed rotating detonation engine," *Combustion and Flame*, Vol. 176, 2017, pp. 12–22. https://doi.org/https://doi.org/10.1016/j.combustflame.2016.09.020.

[18] Hsu, P. S., Slipchenko, M. N., Jiang, N., Fugger, C. A., Webb, A. M., Athmanathan, V., Meyer, T. R., and Roy, S., "Megahertz-rate OH planar laser-induced fluorescence imaging in a rotating detonation combustor," *Opt. Lett.*, Vol. 45, No. 20, 2020, pp. 5776–5779. https://doi.org/10.1364/OL.403199.

[19] Rein, K. D., Roy, S., Sell, B., Caswell, A. W., Hoke, J., Schauer, F., and Gord, J. R., "Time-Resolved *In-Situ* Absorption Spectroscopy of a Hydrocarbon-Air Rotating Detonation Engine using a Fiber-Coupled Tunable Laser System," *54th AIAA Aerospace Sciences Meeting*, 2016. https://doi.org/10.2514/6.2016-1199.

[20] Athmanathan, V., Hoeper, M., Webb, A. M., Wang, R. B., Roy, S., Perkins, H. D., Fugger, C. A., and Meyer, T. R., "Time resolved visualization of liquid jet interaction with H_2-air rotating detonations using MHz rate diesel PLIF," *AIAA SCITECH 2023 Forum*, 2023. https://doi.org/10.2514/6.2023-0573.

[21] Athmanathan, V., Fisher, J. M., Ayers, Z., Cuadrado, D. G., Andreoli, V., Braun, J., Meyer, T., Paniagua, G., Fugger, C. A., and Roy, S., "Turbine-integrated High-pressure Optical RDE (THOR) for injection and detonation dynamics assessment," *AIAA Propulsion and Energy 2019 Forum*, 2019.

[22] Webb, A. M., Crabtree, C., Athmanathan, V., Slipchenko, M., and Meyer, T. R., "KTP Optical Parametric Oscillator for Extended Duration High Repetition Rate NO Planar Laser Induced Fluorescence," *AIAA SCITECH 2023 Forum*, 2023. https://doi.org/10.2514/6.2023-0404.

[23] Haynes, A., Plaehn, E. W., Gejji, R., and Slabaugh, C. D., "Detonation Wave Visualization in a Rocket RDE with Continuous Variation of Fuel Injection Location," *AIAA SCITECH 2023 Forum*, 2023, p. 0928.

[24] Athmanathan, V., Braun, J., Ayers, Z., Fisher, J., Fugger, C. A., Roy, S., Paniagua, G., and Meyer, T. R., "Detonation structure evolution in an optically-accessible non-premixed H2-Air RDC using MHz rate imaging," *AIAA SciTech 2020 Forum*, 2020, p. 1178.